

# Supplemental Material for Rogue Nanowaves: A Route to Film Rupture

James E. Sprittles,<sup>1,\*</sup> Jingbang Liu,<sup>1,†</sup> Duncan A. Lockerby,<sup>2,‡</sup> and Tobias Grafke<sup>1,§</sup>

<sup>1</sup>*Mathematics Institute, Zeeman Building, University of Warwick, Coventry, CV4 7AL, United Kingdom.*

<sup>2</sup>*School of Engineering, University of Warwick, Coventry, CV4 7AL, United Kingdom.*

The Supplemental Material contains: (SM1) a detailed description of the molecular simulations, (SM2) the methods used to solve the stochastic thin film equation and (SM3) a description of the attached videos.

## I. SM1 - MOLECULAR DYNAMICS

Liquid atoms with atomic mass  $6.63 \times 10^{-26}$  kg and solid atoms with atomic mass  $3.24 \times 10^{-25}$  kg are used with the standard Lennard-Jones potential

$$V^*(r_{ij}^*) = 4\alpha_{AB}^* \left[ \left( \frac{\zeta_{AB}^*}{r_{ij}^*} \right)^{12} - \left( \frac{\zeta_{AB}^*}{r_{ij}^*} \right)^6 \right], \quad (1)$$

applied to model their interactions. Here  $r_{ij}^*$  is the distance between atom  $i$  and atom  $j$ ,  $AB$  denotes atom types ( $ff$  for fluid-fluid,  $sf$  for fluid-solid,  $ss$  for solid-solid),  $\alpha_{AB}^*$  is the energy parameter representing the depth of potential wells and  $\zeta_{AB}^*$  is the length parameter denoting the effective atomic diameter. For fluid-fluid interaction, the value of the Lennard-Jones parameters are chosen to be  $\alpha_{ff}^* = 1.67 \times 10^{-21}$  J,  $\zeta_{ff}^* = 0.34$  nm. For solid-fluid interaction,  $\alpha_{sf}^* = 0.7\alpha_{ff}^*$  and  $\zeta_{sf}^* = 0.8\zeta_{ff}^*$ . The cutoff for the Lennard-Jones potential is chosen to be  $7.5\zeta_{ff}^*$ . The solid particles are frozen in the simulations to lower computational cost. The timestep is set to 0.0085 ps and the temperature is set to 85 K. At this temperature, the number density of liquid and vapour are measured in a two phase system to be  $n_l^* = 21.117 \text{ nm}^{-3}$  and  $n_v^* = 5.279 \times 10^{-2} \text{ nm}^{-3}$ . The pressure of the vapour is measured to be  $1.43 \times 10^{-3} \pm 0.5 \times 10^{-3} \alpha_{ff}^*/\zeta_{ff}^{*3}$ .

To prepare the initial condition, a slab of liquid is first created with number density  $n_l^*$  in a periodic box with dimension  $(L^*, L_y^*, h_0^*)$  and equilibrated for  $10^7$  timesteps with a canonical ensemble such that the temperature is kept constant. It is then placed onto a fcc solid plate of number density  $n_s^* = 66.203 \text{ nm}^{-3}$  with dimension  $(L^*, L_y^*, 2.55 \text{ nm})$ . A gap of 0.17 nm is reserved between the liquid and solid, to account for the repulsive force in the Lennard-Jones potential, and its thickness is measured in MD simulation in advance. A block of vapour equilibrated for  $10^7$  timesteps is then placed on top of the liquid, so that the height of the simulation box is 16.5 nm. The average pressure of the equilibrated vapour is measured  $1.48 \times 10^{-3} \alpha_{ff}^*/\zeta_{ff}^{*3}$ . The simulation is then run in the canonical ensemble, with the positions of liquid particles recorded every 500 timesteps. The time-averaged pressure of the vapour remains almost unchanged at  $1.41 \times 10^{-3} \alpha_{ff}^*/\zeta_{ff}^{*3}$  during the simulation. The simulation is performed using open source software LAMMPS [1].

The position of the liquid-vapour interface is determined via the number density and binning method [2]. The number density of each liquid atom is calculated using a sphere of radius 0.51 nm. Note, for atoms close to the solid surface, special care is given in the calculation of number density so that the volume does not include the solid and the gap between solid and liquid. If the number density is higher than  $0.5n^*$  it is categorized as liquid, otherwise it is categorized as vapour. The simulation domain is then discretized into vertical bins, i.e. a  $N_x \times N_y$  grid, and the free surface position in each bin is given by the maximum vertical position of all the liquid atoms inside that bin. For  $L^* = 19.6$  nm we set  $N_x = 50$  and for  $L^* = 80$  nm we set  $N_x = 200$ .  $N_y$  is always set to be 1, as the model is quasi-2D. While this method is accurate away from rupture events, when rupture is approached the film becomes just a layer or two thick this method fails and identifies these film atoms as vapour.

For an accurate measurement of rupture time we consider both the interface position and the solid number density – number density calculated ‘looking up’ from the solid plate. Given a point on the solid plate, instead of a sphere, we use a wedge-shaped volume, and instead of locating the centre of the volume at the point, we locate a vertex of

\*Electronic address: J.E.Sprittles@Warwick.ac.uk

†Electronic address: Jingbang.Liu@Warwick.ac.uk

‡Electronic address: Duncan.Lockerby@warwick.ac.uk

§Electronic address: T.Grafke@Warwick.ac.uk

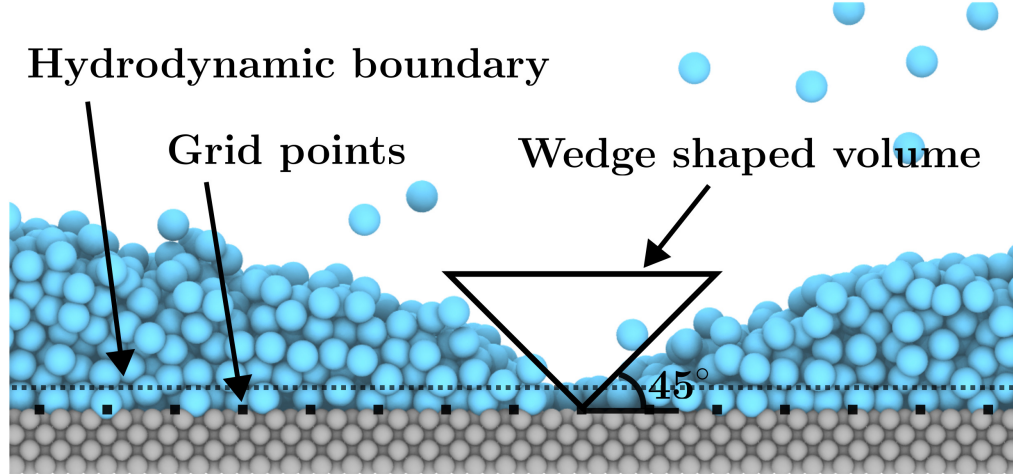


FIG. SM1: Snapshot of MD simulation near film rupture, showing the wedge-shaped volume and grid points used to calculate the solid number density. The hydrodynamic boundary is also highlighted.

the wedge at the point, as shown in Fig. SM1. The angle and the height of the wedge are set to be  $\pi/4$  and 1.36 nm, respectively. If there is one layer of liquid atoms near the solid plate and two vapour atoms in the wedge, the theoretical number density can be calculated to give  $2.411 \text{ nm}^{-3}$ . The solid plate is uniformly discretized into  $N_x$  grid points and solid number density are calculated for these points. We determine that the film has ruptured when, at a point, both interface position reaches 0 and the solid number density is below  $2.411 \text{ nm}^{-3}$ .

Figure SM1 also shows that film heights are measured from a ‘hydrodynamic boundary’, as discussed, e.g., in [3, 4], which was defined to be 0.21 nm above the highest layer of solid atoms. In its simplest form, this accounts for the fact that the liquid isn’t in direct contact with the solid atoms, but is located at some height above. Of course, such effects diminish as the film heights increase.

Transport properties of liquid are also measured in MD simulations using standard methods. The shear viscosity  $\mu^* = 3.1 \times 10^{-4} \text{ kg/ms}$  is calculated via the Green-Kubo method [5]. The surface tension  $\gamma^* = 0.016 \text{ N/m}$  is calculated from the difference between the normal and tangential components of pressure tensor in a simple vapor-liquid-vapor system [6]. The Hamaker constant can be calculated from MD parameters via formula  $A_{AB}^* = 4\pi^2\alpha_{AB}^*(\zeta_{AB}^*)^6 n_A^* n_B^*$  [7]. So the Hamaker constants for liquid-liquid surface interaction and liquid-solid surface interaction are  $A_{ll}^* = 4.5 \times 10^{-20} \text{ J}$  and  $A_{ls}^* = 2.61 \times 10^{-20} \text{ J}$ .

The contact angle is measured in MD with a cylindrical droplet setup [8]. A block of pre-equilibrated liquid with 2046 particles is placed onto the solid substrate and the simulation then run under a canonical ensemble at 85 K for 120000 timesteps until a single droplet is stabilised. The positions of liquid particles are then recorded and the position of the liquid-vapour interface is calculated every 4000 timesteps using the method previously discussed. A circle is then fitted to the mean interface position using the Coope method [9], and the contact angle is measured to be  $93^\circ$ . The slip length is measured to be  $0.46 \pm 0.02 \text{ nm}$ , with method described in [10], which is small compared to  $H^*$  so that no-slip is a reasonable assumption.

Tests were also conducted with a mobile solid, in which the wall atoms were constrained with a harmonic spring and a microcanonical ensemble was used after equilibration. Importantly, using this approach, results for the waiting times were found to be graphically indistinguishable from those obtained with frozen wall atoms.

## II. SM2 - COMPUTATIONAL SOLUTIONS TO THE STOCHASTIC THIN FILM EQUATION

Here, we describe the computational approaches used to solve (i) the STF with constant mobility  $m(h) = h_0^3 + \ell h_0^2$ , which, notably, remains a nonlinear problem, and (ii) the full STF. In both cases, the problem is solved in Fourier space using a pseudo-spectral method which is advantageous due to (i) its accuracy, (ii) its ability to incorporate the periodicity of the domain and (iii) the unambiguous way in which the white noise is cut-off, by projecting it onto the Fourier basis which naturally contains a maximum wavenumber.

*STF with constant mobility* – The advantage of the constant mobility  $m(h) \rightarrow m_0 = h_0^3 + \ell h_0^2$  is that the highest

derivatives in the problem become linear and the noise becomes additive, as opposed to multiplicative, so that:

$$\frac{\partial h}{\partial t} = -m_0 \frac{\partial^4 h}{\partial x^4} + \frac{4m_0 \pi^2}{3} \frac{\partial^2 h^{-3}}{\partial x^2} + \sqrt{2\epsilon m_0} \frac{\partial \eta}{\partial x}. \quad (2)$$

In Fourier space  $(k, t)$  this becomes

$$\begin{aligned} \frac{\partial \hat{h}}{\partial t} &= -m_0 k^4 \hat{h} - a_1(k) \widehat{h^{-3}} + a_2(k) \hat{\eta} \\ &= -m_0 k^4 \hat{h} + G(k, t) + H(k) \hat{\eta}, \end{aligned}$$

where  $\hat{h} = \int_0^1 h e^{-ikx} dx$ ,  $a_1(k) = \frac{4k^2 m_0 \pi^2}{3}$ ,  $a_2(k) = ik \sqrt{2\epsilon m_0}$ ,  $G = a_1 \widehat{h^{-3}}$  and  $H = a_2$ . As the highest derivative is linear, an integrating factor can be used, so that considering a time step from  $t_n$  to  $t_{n+1} = t_n + \Delta t$  gives the *exact* expression

$$\begin{aligned} \hat{h}(t_{n+1}) &= \hat{h}(t_n) e^{c\Delta t} + \\ &e^{c\Delta t} \int_0^{\Delta t} [e^{-c\tau} G(k, t_n + \tau) + e^{-c\tau} H(k) \hat{\eta}] d\tau. \end{aligned}$$

where  $c = -m_0 k^4$ . The simplest treatment of the first term in the integrand follows directly from [11] (termed scheme ETD1) with  $G(k, t_n + \tau) \approx G(k, t_n) \equiv G_n$  in the integral as constant, we arrive at

$$e^{c\Delta t} \int_0^{\Delta t} e^{-c\tau} G(k, t_n + \tau) d\tau \approx G_n (e^{c\Delta t} - 1)/c.$$

For the second term, we note that  $\hat{\eta}$  represents white noise in time, so that the stochastic integral  $e^{c\Delta t} \int_0^{\Delta t} e^{-c\tau} H(k) dW_\tau$  fulfills, via Ito-isometry

$$\begin{aligned} \mathbb{E} \left( e^{c\Delta t} \int_0^{\Delta t} e^{-c\tau} H(k) dW_\tau \right)^2 &= e^{2c\Delta t} \int_0^{\Delta t} \mathbb{E} (e^{-c\tau} H(k))^2 d\tau \\ &= \frac{H(k)^2}{2c} (e^{2c\Delta t} - 1) \end{aligned}$$

and we see that

$$e^{c\Delta t} \int_0^{\Delta t} e^{-c\tau} H(k) dW_\tau = H(k) \sqrt{(e^{2c\Delta t} - 1)/2c},$$

with no approximation. Clearly, once discretized in wavenumber space,  $k$  will be a vector and therefore so will  $c$ . Then, defining  $M_1 = e^{c\Delta t}$ ,  $M_2 = (e^{c\Delta t} - 1)/c$  and  $M_3 = \sqrt{(e^{2c\Delta t} - 1)/2c}$  we arrive at our explicit scheme:

$$h_{n+1} = M_1 \cdot h_n - M_2 \cdot a_1(k) \widehat{h_n^{-3}} + M_3 \cdot a_2(k) \widehat{\eta_n},$$

where  $h_n = h(t_n)$ . After discretization in wavenumber, discrete Fourier transforms are performed with the Fast Fourier Transform algorithm, which we denote FFT. Then, the noise at every time step is given by  $\widehat{\eta_n} = \text{FFT}[N(0, 1)]/\sqrt{\Delta x}$  where  $N$  is a vector of Gaussian random variables with zero mean and unit variance, and  $\Delta x$  is the grid size.

The scheme is implemented into Matlab. Numerical experiments have shown that rupture shapes and times are relatively independent (i.e. indistinguishable graphically, on our plots) if we take 128 grid points and a time step of  $\Delta t = 10^{-7}$ . Such a small step is required to capture the relaxation of sufficiently many wavemodes, with  $c \propto k^4$  creating rapid relaxation of moderate to large wavenumbers.

*Full STF* – When considering the full form of the mobility, the highest derivatives are nonlinear ( $(h^3 \frac{\partial^4 h}{\partial x^4})$ ) and the method presented above fails. The stiffness of the equation makes the time-step constraint on explicit schemes extreme, so we follow the method proposed in [12] by implicitly integrating the deterministic part of the equations, which are still solved in Fourier space using the pseudo-spectral method, using Matlab's built-in ODE15s solver and then adding the noise explicitly using a standard Euler-Maruyama step. Often, the noise is assumed correlated over some length scale and expanded in an orthonormal basis [12, 13]; however, here we choose a simpler method and (i) expand the noise in the Fourier basis and (ii) use the method proposed in [14] to correlate the noise linearly across time steps.

This scheme is considerably more computationally burdensome due to the implicit integration required in between each addition of noise. To lower the burden, we end up ensemble-averaging over less realisations (typically 10, rather than 100 for the scheme above). Also, because  $m \rightarrow 0$  as  $h \rightarrow 0$  means the scheme is ill-posed at  $h = 0$ , we consider breakup to occur once  $h = 0.05$  – results are relatively insensitive to this choice, as disjoining pressure is so strong that breakup is almost guaranteed to follow once at  $h = 0.05$ .

*Validation* – Relatively simple tests for both schemes were performed to confirm that in thermal equilibrium the wave perturbations have the correct standard deviation  $\sigma = \sqrt{\epsilon/12}$  and that with  $m = m_0$  the same results were obtained for ensemble-averaged quantities. A more robust test is to consider the development of the nanowaves from a flat interface, where we can compare to analytic results for the power spectrum  $S(k, t)$ . Specifically, starting from a flat film, the dimensionless version of the results from [7, 15], for a film with  $h = h_0 + \delta h(x, t)$ , is

$$S^2 = \langle |\widehat{\delta h}|^2 \rangle = \epsilon k^2 h_0^3 \omega^{-1} (e^{2\omega t} - 1) \quad (3)$$

where  $\omega = -\frac{k^2}{h_0} [(kh_0^2)^2 - 4\pi^2]$ .

In Fig. SM2, we can see that both schemes reproduce the analytic result well. Naturally, as the analytic result is from a linear theory, the STF with constant mobility works best, and more realisations (100) were also possible with this method. However, the full STF model also gives reassuring results, especially for only 10 realisations, following relatively accurately the trends of the analytic result.

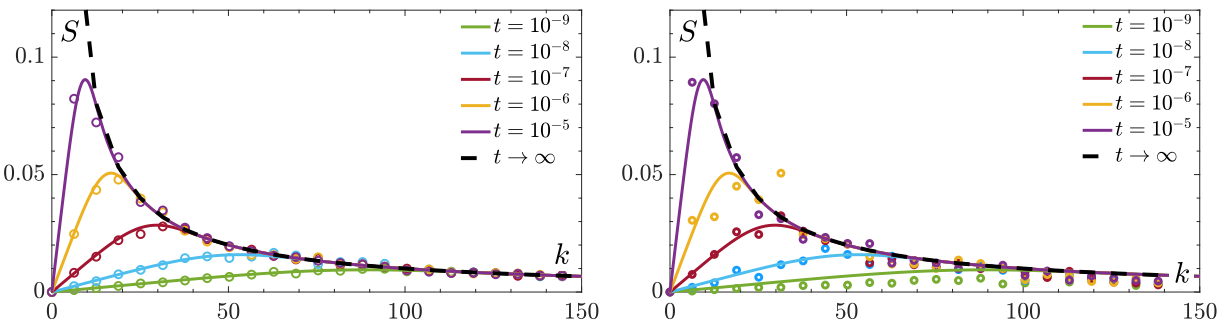


FIG. SM2: Development of the spectrum of thermal waves, starting from a flat interface  $h = h_0 = 2$  at  $t = 0$  with  $\epsilon = 1$ . Ensemble-averaged computational results from the STF with linearized mobility (left, 100 realisations) and full STF (right, 10 realisations) are compared to the analytic solution (3).

*Comparison* – Results for the breakup time  $\langle \tau \rangle$  from the different methods are shown in Fig. SM3 where one can see similar values and trends predicted. Notably, the mobility for the nonlinear system decreases near the breakup point, as  $m \rightarrow 0$  for  $h \rightarrow 0$ , so this phase of the breakup is expected to be slower than the model in which  $m = m_0$  is constant – slightly large  $\langle \tau \rangle$  are indeed seen in Fig. SM3 for the full mobility case. Future analyses could look to improve, and speed-up, the fully nonlinear scheme in order to recover more of the thermal regime, but the indications here are that the method with constant mobility works remarkably well.

### III. SM3 - DESCRIPTION OF THE VIDEOS

The videos show single realisations from the cases shown in Fig. 2 of the Letter, showing rupture in the spinodal and thermal regimes, respectively. The former ( $h_0 = 0.5$ ) is for an initial thickness  $h_0^* = 1.18$  nm and film length  $L^* = 80$  nm and shows rupture in spinodal regime with multiple rupture points. The latter ( $h_0 = 1.14$ ) is for an initial thickness  $h_0^* = 2.69$  nm with film length  $L^* = 80$  nm and shows a rupture typical of that seen within the thermal regime.

Both videos are generated using the open-source package Ovito [16].

---

[1] A. P. Thompson, H. M. Aktulga, R. Berger, D. S. Bolintineanu, W. M. Brown, P. S. Crozier, P. J. in 't Veld, A. Kohlmeyer, S. G. Moore, T. D. Nguyen, R. Shan, M. J. Stevens, J. Tranchida, C. Trott, and S. J. Plimpton, *Computer Physics Communications* **271**, 108171 (2022).  
[2] Y. Zhang, J. Sprittles, and D. Lockerby, *Journal of Fluid Mechanics* **915**, A135 (2021).

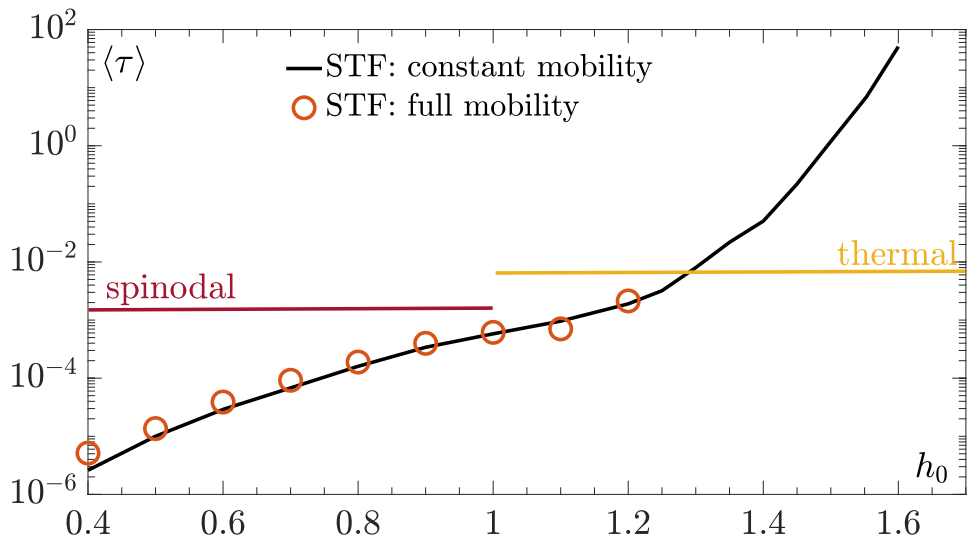


FIG. SM3: Comparison of predicted ensemble-averaged rupture times as computed with the constant mobility  $m(h) = h_0^3 + \ell h_0^2$  (100 realisations) against the full one  $m(h) = h^3 + \ell h^2$  (10 realisations).

- [3] L. Bocquet and J.-L. Barrat, *Physical Review E* **49**, 3079 (1994).
- [4] Y. Zhang, D. A. Lockerby, and J. E. Sprittles, *Langmuir* **37**, 8667 (2021).
- [5] J. M. Haile, I. Johnston, A. J. Mallinckrodt, and S. McKay, *Computers in Physics* **7**, 625 (1993).
- [6] A. Trokhymchuk and J. Alejandre, *The Journal of Chemical Physics* **111**, 8510 (1999).
- [7] Y. Zhang, J. E. Sprittles, and D. A. Lockerby, *Physical Review E* **100**, 023108 (2019).
- [8] J. H. Weijns, A. Marchand, B. Andreotti, D. Lohse, and J. H. Snoeijer, *Physics of Fluids* **23**, 022001 (2011).
- [9] I. D. Coope, *Journal of Optimization Theory and Applications* **76**, 381 (1993).
- [10] Y. Zhang, D. A. Lockerby, and J. E. Sprittles, *Langmuir* **37**, 8667 (2021).
- [11] S. Cox and P. Matthews, *Journal of Computational Physics* **176**, 430 (2002).
- [12] M. A. Durán-Olivencia, R. S. Gvalani, S. Kalliadasis, and G. A. Pavliotis, *Journal of Statistical Physics* **174**, 579 (2019).
- [13] G. Grün, K. Mecke, and M. Rauscher, *Journal of Statistical Physics* **122**, 1261 (2006).
- [14] C. Zhao, D. A. Lockerby, and J. E. Sprittles, *Physical Review Fluids* **5**, 044201 (2020).
- [15] K. Mecke and M. Rauscher, *Journal of Physics: Condensed Matter* **17**, S3515 (2005).
- [16] A. Stukowski, *Modelling and Simulation in Materials Science and Engineering* **18**, 015012 (2009).